Multi-Dimensional Kinetic Simulations of Instabilities and Transport in ExB Devices

IEPC-2015-373／ISTS-2015-b-373

Presented at Joint Conference of 30th International Symposium on Space Technology and Science,
34th International Electric Propulsion Conference and 6th Nano-satellite Symposium
Hyogo-Kobe, Japan
July 4–10, 2015

Johan A. Carlsson,* Igor D. Kaganovich,† Alexander V. Khrabrov,‡ and Yevgeny Raitses§
Princeton Plasma Physics Laboratory, Princeton, New Jersey, 08543, US

Andrei Smolyakov¶
University of Saskatchewan, Saskatoon, Sasktachewan, SK S7N 5E2, Canada

and

Dmytro Sydorenko‖
University of Alberta, Edmonton, Alberta, T6G 2R3, Canada

Abstract: Various ExB devices such as Hall thrusters, helicon thrusters, Penning and magnetron discharges are subject to numerous instabilities that yield anomalous electron transport and affect operation of these devices. To understand details of anomalous electron transport in ExB devices we have performed multi-dimensional kinetic simulations of plasma processes in a number of ExB discharges. Results of simulations are compared with experimental finding and fluid simulations. The LSP (Large-Scale Plasma) PIC-MCC code has been substantially modified to simulate several ExB configurations including Hall Thruster and Penning discharge. To enable robust simulations of these discharges, we implemented a new electrostatic solver using the PETSc library interface; we added comprehensive collision models based on anisotropic scattering, implemented electron emission algorithms from EDIPIC code and modified the external electric circuit model. Hence, we call the customized code PPPL-LSP. As a result the code can be run on hundreds of processor cores, and simulations can resolve fast electron processes as well as reach steady state (on ion-time scale) without scaling of cross sections or reducing ion mass. We have performed extensive verification and validation of the modified code. In particular, various instabilities in ExB devices were simulated for Penning and magnetron discharges. Initial three-dimensional simulations of the cylindrical Hall thruster were also performed.

*Computational Expert, Plasma Science and Technology Department, jcarlsso@pppl.gov
†Principal Research Physicist, Plasma Science and Technology Department, ikaganov@pppl.gov
‡Researcher, Plasma Science and Technology Department, akhrabro@pppl.gov
§Principal Research Physicist, Plasma Science and Technology Department, yraitses@pppl.gov
¶Professor, Department of Physics and Engineering Physics, andrei.smolyakov@usask.ca
‖Research Associate, Department of Physics, sydorenk@ualberta.ca

Nomenclature

ϱ_e = electron Larmor radius
ν_{en} = electron-neutral collision frequency
ω = mode angular frequency
$\mathbf{k}$ = mode wave vector
c_s = sound speed
x = radial location
z = axial location
$\mathbf{E}$ = electric field
$\mathbf{B}$ = magnetic field
ϕ = electrostatic potential
e = elementary charge
M = ion mass
ω_{ci} = ion cyclotron angular frequency
ω_{ce} = electron cyclotron angular frequency
ω_{LH} = lower-hybrid angular frequency
f = frequency

I. Introduction

An effort is underway at the Princeton Plasma Physics Laboratory (PPPL) to modify, improve, verify and validate three Particle-In-Cell (PIC) codes for low-temperature plasma (LTP) and beam applications. Of particular interest to us is the PPPL conventional [1] and cylindrical [2] Hall thruster experiments (HTX) general for coherent structures [3, 4] in Hall thrusters in particular. Similar simulations have been performed by Taccogna [5], Matyash [6], Boeuf [7] and Cappelli [8]. The three PIC codes used by us are EDIPIC [9] (University of Saskatchewan / University of Alberta / PPPL), WARP (Lawrence Berkeley National Laboratory) and the commercial code LSP, which provides source code to licensees. All three codes are parallelized using MPI to run on dozens to hundreds of processors and have each been used to produce physics results published in several peer-reviewed journal papers. The different codes all have individual strengths and weaknesses. EDIPIC is well-validated for thruster and other LTP applications, but can currently only numerically resolve one spatial dimension. WARP can perform one- and two-dimensional simulations, but is primarily a beam code. LSP is the most versatile one and can be used for one-, two- and three-dimensional simulations in Cartesian, cylindrical and spherical geometries, but has been relatively little used for LTP simulations. The development and validation of all three codes benefits from the broad computational, experimental and analytical plasma expertise available at PPPL. For code validation, the flexible and well-characterized PPPL Low-Temperature Plasma Experiment (LTPX) is a particularly valuable resource.

This paper focuses on recent work to improve, benchmark and validate LSP for LTP applications, including thrusters and power electronics. The benchmarking has been done against the EDIPIC code for glow-discharge and magnetron simulations. The glow discharge is a suitable target for benchmarking because it exposes even minor deficiencies of collision models, and for validation because detailed results from a well-characterized experiment are available [10]. The goal of the benchmarking / validation exercise is to ensure the correctness of LSP for one-dimensional LTP simulations, so that one can be more confident in two- and three-dimensional results.

The one-dimensional glow-discharge benchmarking / validation will be succeded by two- and three-dimensional LSP simulations of a Penning discharge, which will be validated against LTPX. This LTPX validation has not yet begun, but some preliminary results from the simulations are presented below. Complete results will be presented in future publications.

II. Simulations of a Penning discharge

A. One-dimensional simulations of a Penning discharge

The initial Penning-discharge simulations were set up for a reduced one-dimensional geometry with the resolved x direction corresponding to the radial direction of an actual device. A narrow 13-mA, 10-eV electron beam is injected around $x = 0$ in the z (axial) direction into partially ionized helium in a domain bounded by metal walls at $x = \pm 1/2cm$. Gas pressure is 200 μTorr. Initial electron temperature is 10 eV, initial ion temperature is room temperature (25.2 meV) and intial densities are $5 \times 10^{11} cm^{-3}$. To resolve the Debye radius spatially and the plasma oscillation temporally, 1000 (10 μm) cells and a 5 ps time step are used. A homogeneous magnetic field is applied in the z direction with strength chosen to fully magnetize the electrons (spatially and temporally), but leave the helium ions only very weakly magnetized. Because the domain size is smaller than a typical experimental device, the magnetic field was increased in the simulations to keep a realistic ratio of size to Larmor radius. For most of the simulations 100 Gauss was used, with the domain size corresponding to about half of an ion Larmor radius and 20 electron Larmor radii. The numerically unresolved y and z directions have electric field components identical to zero ($E_x = -d\phi/dx$, $E_y = E_z = 0$) and periodic boundary conditions for particles. As a consequence, the electron beam injected at $x = -1/2cm$ wraps around when it reaches $x = +1/2cm$ and the axial current is a multiple of the injected current.

For the baseline gas pressure (200 μTorr) the collision time is about $10^5/s$, typical of experimental conditions. The collision models used were charge exchange for the ions and for the electrons elastic and inelastic collisions with neutrals. Ionization and secondary-electron emission were neglected. For this simulation set up it takes approximately 5 μs for the axial current to level off. As can be seen in Fig. 1a, a deep potential develops to drive leakage current in the radial direction to balance the injected current in the axial direction. The collision time is longer than the ion transit time, and ions are therefore adiabatically trapped in the potential well. The IEDF is nearly Maxwellian (not shown) and the Boltzmann relation can be used to approximate the ion density, as shown in Fig. 1b. From Ohm's law and the ion Boltzmann relation, one

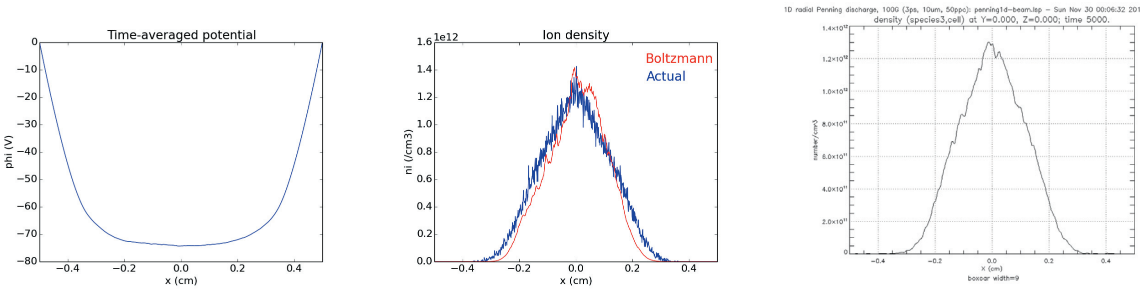

Figure 1. a) Time-averaged electrostatic potential vs. radial coordinate (x). b) Ion density given by Boltzmann relation (red) compared to directly-computed one (blue). c) Electron density from simulation, consistent with Eq. 1.

gets:

$$J(x) = \int_0^x Q(x')dx' = \sigma\left(E - \frac{dP_e/dx}{e}\right) = \sigma E\frac{T_e + T_i}{T_i} = \sigma(T_e + T_i)\frac{1}{n}\frac{dn}{dx} \sim dn/dx\,, \tag{1}$$

so that if the current density is constant, then the density profile will be linear, in agreement with the almost triangular electron-density profile shown in Fig. 1c. The interior plasma is quasi-neutral (not shown).

To estimate the importance of anomalous versus classical transport, we compared simulations results from the 200 μTorr base case with simulations at lower gas pressures: 100 μTorr and 0 μTorr, respectively. As can be seen in Fig. 2a, at lower pressures the potential well deepens to maintain the radial leakage current that must balance the axially injected current at steady state. This is consistent with the expected increase

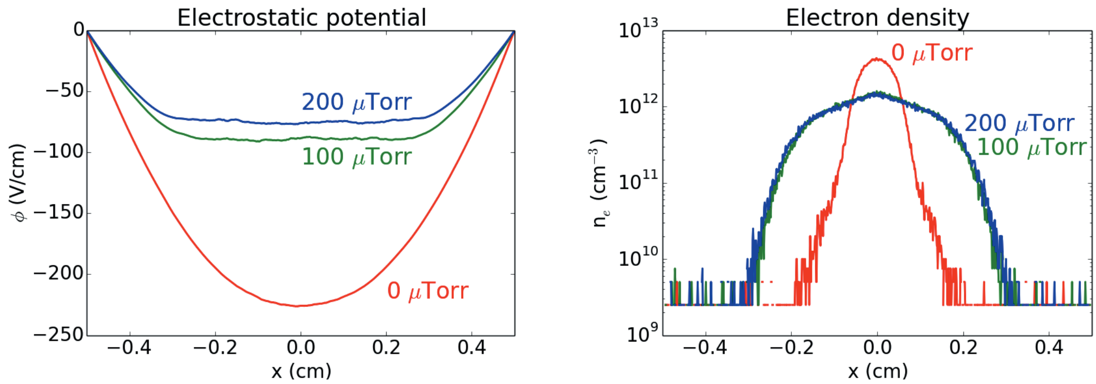

Figure 2. a) Electrostatic potential vs. radial coordinate (x) for three different values of gas pressure. b) The corresponding electron density profiles (notice the logarithmic ordinate).

of the relative importance of anomalous transport with decreasing gas pressure. At 200 μTorr, classical transport is larger than the anomalous one, but the latter does not become negligible until gas pressure is increased to around a mTorr.

The ions and electrons of the simulated system start rotating in the counter-clockwise direction, which corresponds to the $E \times B$ and diamagnetic drift directions for the electrons, and the $E \times B$ drift direction for the ions. The electrons rotate two orders of magnitude faster than the ions. Conservation of generalized momentum for the ions in the y direction gives:

$$Mv_y = eB\Delta x/c \Rightarrow v_y = \omega_{ci}\Delta x\,, \tag{2}$$

where Δx is the displacement from the initial location. Correspondingly, the ion rotation is $\langle nv_y\rangle \sim -n\omega_{ci}x$ and the ions rotate as a rigid body with a well-defined rotation frequency. Approximate rigid-body rotation (at different velocities) is indeed seen in the simulations for both ions and electrons, but not shown here. To identify the mode responsible for the anomalous transport and plasma rotation, magnetic field, ion mass and gas pressure were independently changed. It was found that mode frequency ω scaled as $\omega \sim B$ and

$\omega \sim M^{-1/2}$, consistent with the lower-hybrid mode,

$$\omega = \omega_{LH} = \sqrt{\omega_{ce}\omega_{ci}}\,. \tag{3}$$

Fig. 3 shows the frequency spectrum of the electrostatic potential multiplied with electron density, since this product is particularly interesting, being proportional to the anomalous electron flux. As can be seen, the

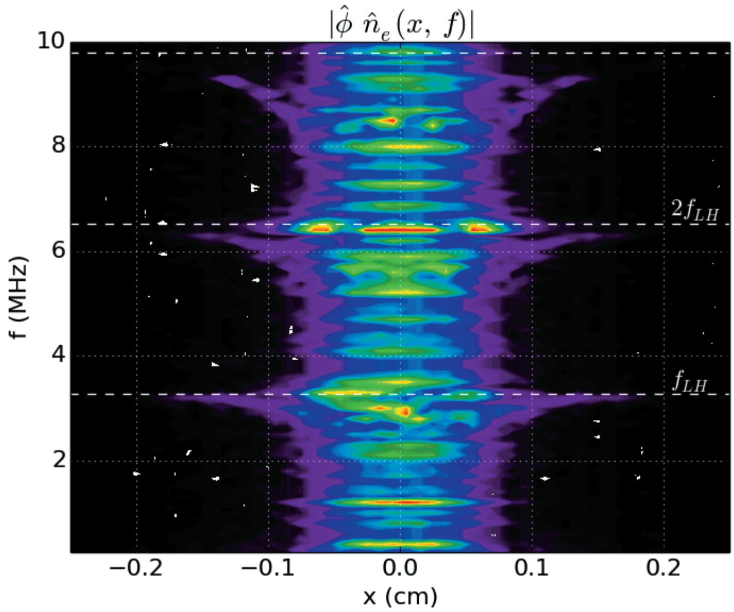

Figure 3. Frequency spectrum for product of electrostatic potential and electron density for zero-pressure case. Red is the largest amplitude and black is zero.

lower-hybrid mode has a large amplitude in the core plasma, as evidenced by the elongated peak around $x = 0$ and frequency $f = \omega_{LH}/\pi\,(= 2f_{LH})$. For higher pressures, additional modes are seen, but the lower-hybrid one is the only that is always present for various values of gas pressures, magnetic field and ion mass.

B. Two-dimensional simulations of a Penning discharge

The two-dimensional simulations are an extension of the one-dimensional simulations described above. To avoid potential issues with injecting a beam into the origin of a cylindrical coordinate system, these intial two-dimensional simulations are of a square cylinder, $-0.5cm \leq x, y \leq 0.5cm$, bounded by metal on all four sides. To resolve the Debye sphere and plasma oscillation, 500×500 (20 μm) cells and a 5 ps time step are used. Compared to the one-dimensional case, the beam current is increased 80 mA, with homogeneous current density for $-0.01cm \leq x, y \leq 0.01cm$ and zero outside.

In the one-dimensional simulations, the artificial restriction that the azimuthal wave number must be zero severly limited the number of available modes. In the two-dimensional simulations, this restriction is lifted and one can thus expect more modes to become unstable and drive anomalous transport. The two-dimensional simulations exhibit much stronger anomalous transport than the one-dimensional simulations. Even a very weak potential well of 1 to 2 volts is sufficient to drive a leakage (cross-field) current that balances the injected current. Ions are not confined and are lost to the walls on the time scale of the ion transit time (device size divided by ion thermal speed) of about 1 μs. The beam injection of electrons is two orders of magnitude too small to balance the losses and the simulations are therefore typically run to about 2 μs.

Like in the one-dimensional simulations, both ions and electrons rotate in the counter-clockwise direction. The rotation velocities are roughly proportional to the radius, corresponding to rigid-body rotation, with the electrons rotating about two orders of magnitude faster than the ions. Because of the very peaked density, the electron diamagnetic drift is estimated to be faster than the $E \times B$ drift and is in rough agreement with the observed rotation frequency of 2–2.5 MHz. To help determine whether the rotation is diamagnetic or $E \times B$, we plot the current streamlines on top of potential and pressure contours at the final time step in Fig. 4. As is clearly seen, the electron pressure shows much better agreement with the current, supporting the

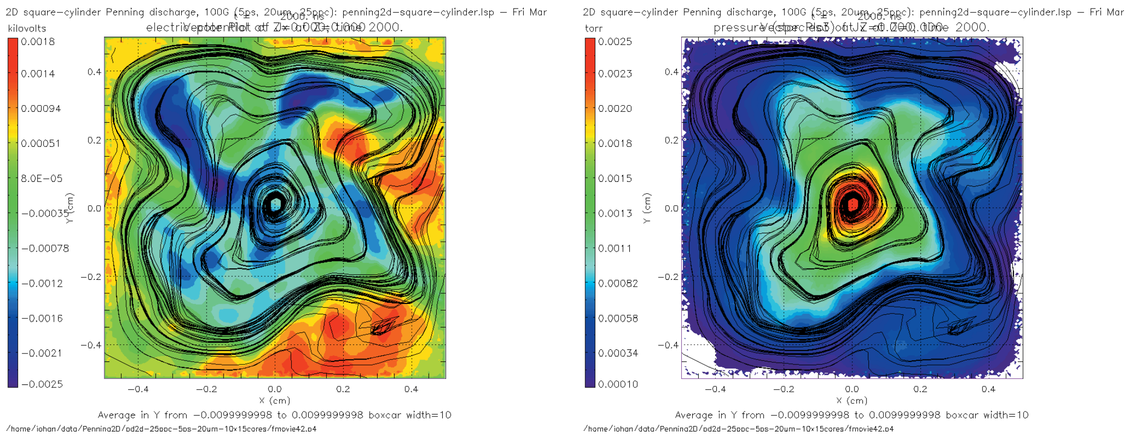

Figure 4. a) Current streamlines on top of potential contours at 2 μs. b) Current streamlines on top of electron-pressure contours at 2 μs.

idea that the current is primarily due to diamagnetic drift, not $E \times B$ drift. Note the spoke-like appearance of the rotating structure visible in both potential and pressure plots.

The radial current exhibits bursts at the spoke frequency, see Fig. 5. It is possible to correlate the bursts

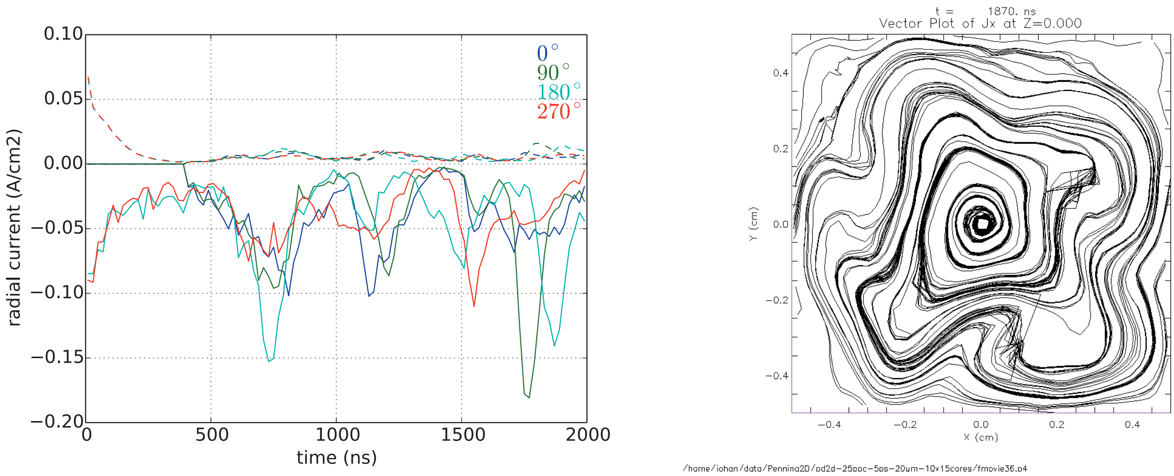

Figure 5. a) Radial current vs. time at four different locations for electrons (solid graphs) and ions (dashed). b) Snapshot of current streamlines at time of last current burst at 1870 ns.

with a spoke sweeping by. When a current burst occurs, one would expect current stream lines from the interior plasma to connect with the wall. This is demonstrated for the last burst of Fig. 5, at 1870 ns and 180°. The corresponding streamline plot at 1870 ns to the right shows streamlines running parallel to the wall at the top (90°) and the bottom (270°), resulting in minimal radial current at those locations. At the 0° location (x=+0.5cm, y=0) some current streamlines connect, but particularly at 180° (x=-0.5cm, y=0). The former shows up as an intermediate level of radial current and the latter as a burst, in good agreement with Fig. 5a.

A more more thorough analysis will be presented when the two-dimensional Penning-discharge simulations are completed.

III. Two-dimensional diocotron and magnetron simulations

As was demonstrated by simulations performed by Boeuf [7], at low pressures annular $E \times B$ devices can have regions where the electron density is much larger than the ion density, possibly making them susceptible to diocotron instabilities [11, and references therein]. To investigate this regime, we have initiated PPPL-LSP simulations of a stabilized diocotron experiment [11]. It is a simulation in annular geometry, performed in cylindrical (r, θ) coordinates, with a pure electron plasma confined by a strong axial magnetic field between an inner cathode and outer grounded anode. Theory predicts that in this configuration the diocotron instability becomes completely stabilized for all azimuthal mode number for sufficiently large radial electric fields [11]. Fig. 6 shows a simulation of a diocotron instability with high azimuthal mode number that is nonlinearly saturated by electron trapping in a radial electric field generated by putting a -2 kV bias on the inner annulus. The axial magnetic field is 1 kGauss.

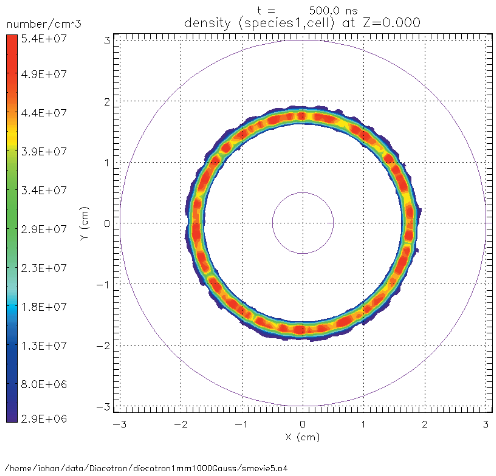

Figure 6. Fully stabilized diocotron mode.

The PPPL-LSP code has also been used for other applications, exercising physics model such as ionization and ion electron secondary emission, that will be enabled for future Penning-discharge simulations. An example is a two-dimensional Cartesian simulation of a magnetron with a power-electronics application [12]. Fig. 7a shows one of the magnetic field configurations used for performance optimization of the device. Fig. 7b shows the resulting ion-density contour with a maximum due to impact ionization in the cathode fall from secondary electrons.

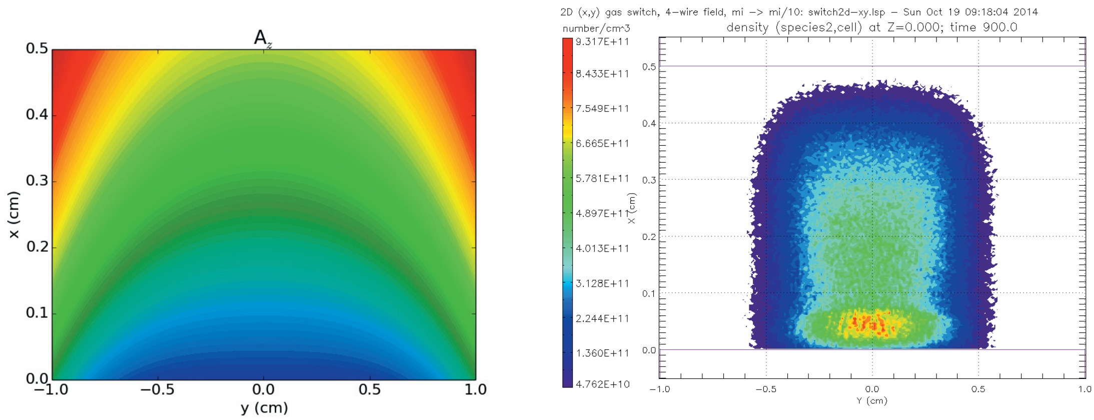

Figure 7. a) Stream function (axial component of vector potential) of magnetic field used for two-dimensional magnetron simulation. Cathode at the bottom and anode at the top. b) Corresponding ion density.

IV. Code modifications, benchmarking and validation

The Large-Scale Plasma (LSP) PIC code is a commercial code that is actively being used for many applications, including beam physics. It has several attractive features: it comes with source code so it can be scrutinized and even modified and recompiled, and it is relatively easy to learn to use. However, for low-temperature plasma applications we encountered several issues that we have now resolved. We refer to this improved version of the code as PPPL-LSP. PPPL-LSP allows us to perform large two-dimensional and small three-dimensional simulations of low-temperature plasma in Cartesian and cylindrical coordinates. It scales well to about one thousand processor cores and if and when needed, we can increase scalability by an order of magnitude by removing two known and well-understood bottlenecks in the code with moderate effort.

The major code improvement of PPPL-LSP is the addition of a direct electrostatic (ES) field solver. The standard version of LSP has an iterative ES solver, using either the Alternating-Direction Implicit (ADI) or the Successive Over Relaxation (SOR) algorithms. The ADI ES solver is fast and works well for one-dimensional simulations. However, for two- and three-dimensional simulations, we were unable to get it to fully converge and the ES field suffered accumulating residual errors (essentially artificial charge build up) until the simulation results became unphysical. Considerable effort went into tuning the various parameters that affect the performance of both the ADI and SOR ES solvers, but to no avail. It was then decided to implement a robust, direct ES solver that solves the discretized Poisson equation exactly (within rounding errors due to finite floating-point precision). The new solver used an existing interface to the PETSc solver library, which was upgraded to the latest version, to call a direct-solver library, either MUMPS or SuperLU. MUMPS is faster, but SuperLU more robust and both are now routinely used.

An example of the problems encountered with the ADI ES solver in two-dimensional simulations is shown in Fig. 8. A very simple simulation in Cartesian coordinates was performed of sheath formation in a homogeneous plasma bounded by grounded metal walls. With the ADI ES solver we were unable to achieve the recommended tolerance of 10^{-12} despite considerable effort spent on performance tuning. The best possible tolerance was 10^{-8}, which resulted in a growing field residual that eventually caused the solution to become unphysical with spurious oscillations.

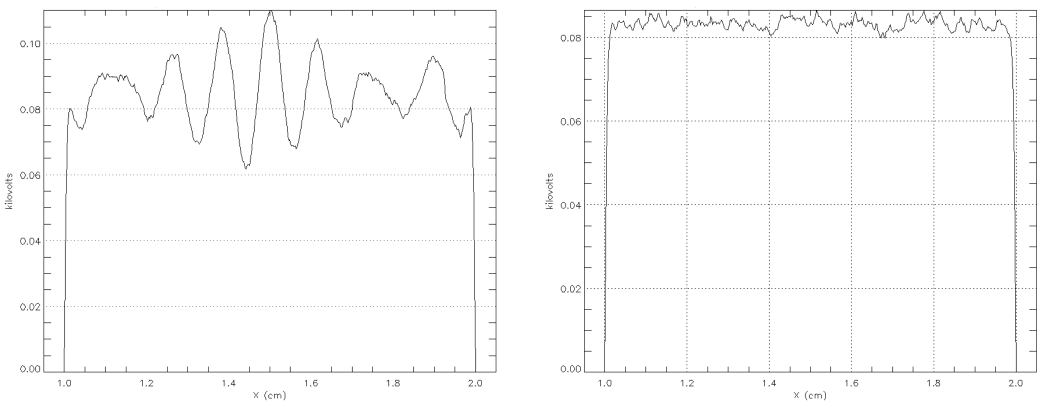

Figure 8. a) Electrostatic field computed with ADI ES solver exhibits spurious oscillations. b) New MUMPS ES solver computes the field correctly.

To enable simulations of plasma devices with a prescribed current flowing through them, an algorithm for a new external-circuit model was developed and implemented. The existing circuit model was numerically unstable and often created spurious current spikes that terminated the simulations. To resolve a problem with avalanching number of macro particles when secondary-electron emission (SEE) was turned on, all the available code options were explored, but failed to give a satisfactory result. A rejection-method algorithm for SEE was therefore implemented that gives the newly created particles the same numerical weight as the existing ones of the same physical species. We found it necessary to impose this restriction to get the collision models to work properly and therefore implemented a rejection-method also for injection of charged particles. The collision models were also tested, modified (charge exchange) and extended (new anisotropy models [13] for elastic, excitation and ionization). Some minor generalizations of the code were made to allow e.g. beam injection in a numerically unresolved direction. Several minor bug fixes in various parts of the code were also done.

A set of Python scripts were also developed to complement the existing P4 post processor for plotting and analyzing simulation data in more detail.

A validation and benchmarking exercise of the codes PPPL-LSP and EDIPIC is currently being completed for a simulation of a glow-discharge experiment. A divide-and-conquer approach was used for benchmarking the codes where the full problem was divided into sub-problems that were individually benchmarked. An example of this is shown in Fig. 9 for injection of a 25-eV electron beam into a helium plasma. The two

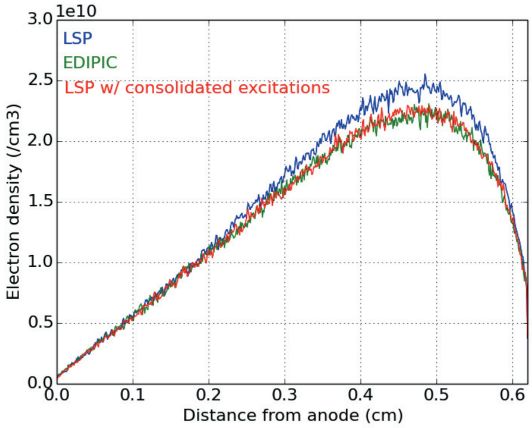

Figure 9. Comparison of electron-density profiles computed by the PPPL-LSP and EDIPIC codes for electron-beam injection into helium gas.

codes initially differed by up to 15%. Because of the simplicity of the simulation, the cause was readily identified as being due to different models for excitation collisions in the two codes. A small fraction of the beam electrons in the LSP simulation excited helium atoms to higher energy levels and were subsequently cooled to around an eV. This small population of cool electrons were better confined and contributed to an increased density. When the cross-section table used for LSP was modified to consolidate six separate excitation cross sections into a single, energy-weighted one, the discrepancy was completely removed, as can be seen in Fig. 9. Dozens of similarly simplified, synthetic benchmarks have been performed for the two codes leading up to the full validation exercise utilizing all the individually tested physics models in each code. The results will be presented in the near future in a separate publication.

V. Conclusion

The EDIPIC and PPPL-LSP PIC codes are being modified and validated for low-temperature plasma simulations. PPPL-LSP is now capable of accurately simulating $E \times B$ devices in two and three spatial dimensions using Cartesian and cylindrical coordinate systems. A rotating spoke-like structure is seen in both one- and two-dimensional simulations of a Penning discharge. In the one-dimensional case the mode responsible was indentified as the lower-hybrid instability.

Acknowledgments

The research presented in this paper was funded by AFOSR.

References

[1]Raitses, Y., and Fisch, N. J., "Parametric investigations of a nonconventional Hall thruster," *Physics of Plasmas*, Vol. 8, 2001, p. 2579; Raitses, Y., Keidar, M., Staack, D., and Fisch, N. J., "Effects of Segmented Electrodes in Hall Current Plasma Thrusters," *Journal of Applied Physics*, Vol. 92, 2002, p. 4906.

[2]Smirnov, A., Raitses, Y., and Fisch, N. J., "Experimental and theoretical studies of cylindrical Hall

thrusters," *Physics of Plasmas*, Vol. 14, 2007, p. 057106.

[3]Raitses, Y., *et al.*, in Proceedings of IEPC 2013.

[4]Smolyakov, A., *et al.*, in Proceedings of IEPC 2013.

[5]Taccogna, F., Longo, S., Capitelli, M., and Schneider, M., "Anomalous Transport induced by Sheath Instability in Hall Effect Thrusters," *Applied Physics Letters*, Vol. 94, 2009, p. 251502.

[6]Matyash, K., Schneider, R., Kalentev, O., Raitses, Y., and Fisch, N. J., "Numerical investigations of a cylindrical Hall thruster," in Proceedings of IEPC 2011.

[7]Boeuf, J.-P., "Rotating structures in low temperature magnetized plasmas – insight from particle simulations," *Frontiers in Physics*, Vol. 2, 2014, p. 74.

[8]Meezan, N. B., and Cappelli, M. A., "Kinetic study of wall collisions in a coaxial Hall discharge," *Phys. Rev. E*, Vol. 66, 2002, p. 036401.

[9]Sydorenko, D., "Particle-in-cell simulations of electron dynamics in low pressure discharges with magnetic fields," Ph.D. Dissertation, Department of Physics and Engineering Physics, University of Saskatchewan, 2006.

[10]Den Hartog, E. A. and Doughty, D. A., and Lawler, J. E., "Laser optogalvanic and fluorescence studies of the cathode region of a glow discharge", *Physical Review A*, Vol. 38, 1988, pp. 2471–2491.

[11]Rosenthal, G., Dimonte, G., and Wong, A. Y., "Stabilization of the diocotron instability in an annular plasma," *Physics of Fluids*, Vol. 30, 1987, pp. 3257–3261.

[12]`http://scitation.aip.org/content/aip/magazine/physicstoday/news/10.1063/PT.5.5022`

[13]Khrabrov, A. V., and Kaganovich, I. D., "Electron scattering in helium for Monte Carlo simulations," *Physics of Plasmas*, Vol. 19, 2012, p. 093511; Okhrimovskyy, A., Bogaerts, A., and Gijbels, R., "Electron anisotropic scattering in gases:A formula for Monte Carlo simulations," *Phys. Rev. E*, Vol. 65, 2002, p. 037402.